Matter-First Spin Foams: Bivector Simplicity, Lorentzian Boosters, and a Tensor-Network EPRL Vertex

Ginanjar Utama
ginanjar.utama@gmail.com

June 27, 2026

Abstract

A previous paper proposed a matter-first route to loop quantum gravity: interaction vertices define the graph, fermion-line segments carry local $\mathrm{SL}(2,\mathbb{C})$ frames, and geometry is reconstructed from the resulting spacetime-algebra comparators. Its central open gap was the relation between those matter-built bivectors and the simplicity-constrained boundary data of spin-foam dynamics. This paper closes that kinematical gap and adds a finite-cutoff vertex algorithm. First, we express the EPRL linear simplicity constraint in the invariant plane of the bivector classification $B^2 = s + pI$: up to the standard sign and normalisation conventions for $\mathrm{SL}(2,\mathbb{C})$ Casimirs, the EPRL embedding $Y_\gamma : j \mapsto (\rho, k) = (\gamma j, j)$ selects a ray $p/s = 2\gamma/(\gamma^2 - 1)$. Second, we sharpen the closure bridge: the area-vector closure condition at a tetrahedron is equivalent to the Minkowski polygon inequality, and this is exactly the condition that the four-valent intertwiner space be non-empty. Thus classical closure and quantum admissibility are two presentations of the same Gauss constraint. Third, we construct the Lorentzian vertex from the same data: the boost sector is represented by principal-series generators certified by the $\mathfrak{so}(1,3)$ algebra and Casimirs, and the node booster B_4^γ is evaluated as a radial boost integral. Finally, by absorbing each booster and intertwiner into a rank-four node tensor, the finite-cutoff EPRL four-simplex amplitude becomes a tensor-network contraction on K_5 rather than an explicit state sum. The result is not a continuum limit; it is a reproducible bridge between the matter determinant, bivector simplicity, and a computational Lorentzian EPRL vertex.

1 Introduction

The previous paper in this sequence, now posted as ai.viXra:2606.0064 [1], developed a matter-first version of loop quantum gravity inspired by Penrose's combinatorial spacetime [2] and Altaisky's locally Lorentzian matter-spin-network construction [3]. The basic move was to start not from a pre-existing lattice of geometry, but from interaction events and fermion-line segments. Each line carries an $\mathrm{SL}(2,\mathbb{C})$ frame; comparing neighbouring frames gives the discrete connection; loop curvature is the bivector logarithm of the holonomy in the spacetime algebra $\mathrm{Cl}(1,3)$ [18, 19]; and the bilinear Grassmann action gives an exact determinant $Z = \det D$. Gauge invariance then reduces the determinant to a function of cycle-space holonomies, with $b_1 = |E| - |V| + 1$ independent cycles.

That construction deliberately stopped before the spin-foam vertex. It produced a matter-induced geometry and an induced field equation [20], but the elementary grade-two areas were not yet constrained by the simplicity conditions that select gravitational bivectors inside the larger topological BF phase space [6]. Nor did it provide the Lorentzian EPRL vertex amplitude. The present paper supplies that missing bridge.

The contribution is threefold.

1. **Bivector simplicity.** The boost-rotation split of a curvature bivector B gives two invariants, $s = \langle B^2\rangle_0$ and $pI = \langle B^2\rangle_4$. The EPRL map $Y_\gamma : j \mapsto (\rho, k) = (\gamma j, j)$ carries the same invariant pair, modulo the usual sign and additive conventions for $\mathrm{SL}(2,\mathbb{C})$ Casimirs. In the classical limit, the linear simplicity constraint $\vec{K} = \gamma\vec{L}$ is a ray in the (s, p) plane.

2. **Closure as admissibility.** At a tetrahedron, area-vector closure is possible precisely when the four face areas obey the Minkowski polygon inequality. The same inequality is the condition for a non-empty four-valent intertwiner space. This identifies the geometric closure constraint with the quantum Gauss constraint at the node.

3. **A finite-cutoff Lorentzian vertex engine.** The $\mathrm{SL}(2,\mathbb{C})$ booster is built from principal-series generators whose commutators and Casimirs are explicitly checked. The resulting B_4^γ is fused with the four-valent intertwiner into a node tensor, so the four-simplex amplitude is evaluated as a tensor network on K_5. This makes the same graph cycle structure visible on both sides: holonomies in the matter determinant and magnetic indices in the spin-network evaluation.

We will be careful about scope. The paper does not prove a continuum limit, does not claim that a single vertex reproduces general relativity, and does not supersede specialised high-performance EPRL codes. The claim is narrower and, for the present programme, more useful: the matter-built $\mathrm{Cl}(1,3)$ bivectors, the EPRL simplicity map, the Lorentzian booster, and the efficient four-simplex contraction can be written in one consistent language and verified in a reproducible finite-cutoff implementation.

2 Simplicity as bivector classification

2.1 The invariant plane

Let $B \in \mathrm{Cl}^+(1,3)$ be a Lorentz bivector, decomposed into boost and rotation parts as

$$B = \vec{K}\cdot\hat{\boldsymbol{\sigma}} + \vec{L}\cdot I\hat{\boldsymbol{\sigma}}, \qquad \hat{\sigma}_i = \gamma_i\gamma_0, \tag{1}$$

where $\hat{\sigma}_i^2 = +1$ and $I\hat{\sigma}_i$ are the rotation bivectors. Then

$$B^2 = s + pI, \qquad s = |\vec{K}|^2 - |\vec{L}|^2, \qquad p = 2\vec{K}\cdot\vec{L}. \tag{2}$$

These are the two Lorentz invariants used in [1] to classify elliptic, hyperbolic, parabolic, and loxodromic holonomies.

The EPRL model imposes linear simplicity weakly through the embedding

$$Y_\gamma : \quad j \longmapsto (\rho, k) = (\gamma j, j), \tag{3}$$

from an SU(2) spin into a unitary principal-series representation of $\mathrm{SL}(2,\mathbb{C})$ [5, 4, 10]. Classically this corresponds to

$$\vec{K} = \gamma\vec{L}. \tag{4}$$

Substitution into (2) gives the basic geometric reading of the Barbero–Immirzi parameter.

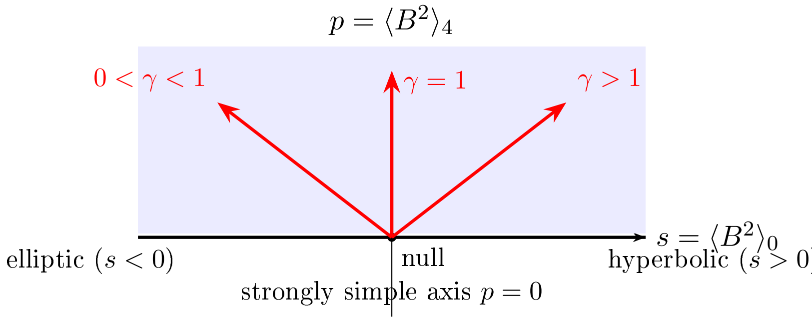

Figure 1: Linear simplicity as a ray in the bivector invariant plane. Strong diagonal simplicity is the axis $p = 0$; finite EPRL γ selects a fixed loxodromic ray.

Proposition 1 (EPRL simplicity is a ray in the invariant plane)**.** *For boundary data satisfying* (4)*,*

$$s = (\gamma^2 - 1)|\vec{L}|^2, \qquad p = 2\gamma|\vec{L}|^2, \tag{5}$$

so the bivector lies on the ray

$$\frac{p}{s} = \frac{2\gamma}{\gamma^2 - 1} \tag{6}$$

in the (s, p) *classification plane. With* $(\rho, k) = (\gamma j, j)$*, the principal-series invariants* $(\rho^2 - k^2, 2\rho k)$ *reproduce the same pair, up to the fixed sign and additive constants used by different Lorentz-Casimir conventions.*

Remark 1 (Conventions)*.* There are two common sources of sign shifts. First, some authors use $C_1 = k^2 - \rho^2$ while others use $C_1 = \rho^2 - k^2 + 1$. Second, the sign of $\vec{J} \cdot \vec{K}$ depends on the orientation chosen for the boost generator. These choices do not affect the content of Proposition 1: the EPRL label $(\gamma j, j)$ fixes the same two-dimensional invariant data as the spacetime-algebra bivector.

2.2 Strong and weak simplicity

The companion paper used elementary tetrad areas of the form

$$F^{[ij]} = \tfrac{1}{2} e^{[i,j]} \wedge e^{[i+1,j]}, \tag{7}$$

which are simple blades by construction: $F \wedge F = 0$. This is strong diagonal simplicity. The EPRL bivector at finite γ is different. It is not generally a strongly simple blade in the sense $p = 0$; rather, it satisfies the linear simplicity relation (4) weakly at the quantum level. Thus the correct bridge is not that every finite-γ EPRL bivector is strongly simple. The bridge is that both the matter-built blade and the EPRL representation label are controlled by the same invariant pair, with γ specifying how the weakly imposed quantum constraint tilts the data away from the strongly simple axis.

3 Closure equals admissibility

The next condition is closure. At a boundary tetrahedron τ, the four face area-vectors must sum to zero,

$$\sum_{f \subset \partial\tau} \vec{A}_f = 0. \tag{8}$$

This is the classical Gauss constraint. In the bivector language one may write the same condition as a closure of the four appropriately transported face bivectors; in this section we focus on the area-vector content, because that is exactly what is quantised by the four-valent intertwiner.

Lemma 1 (Area closure and the polygon inequality)**.** *Let $A_1, \dots, A_4 \geq 0$ be four face areas. There exist four vectors in $\mathbb{R}^3$ of these lengths whose sum is zero if and only if*

$$A_i \leq \sum_{j \neq i} A_j \qquad (i = 1, \dots, 4). \tag{9}$$

This is the four-face version of Minkowski's theorem for convex polyhedra [7, 8].

On the quantum side, a four-valent node with spins $j_1, \dots, j_4$ carries an intertwiner precisely when

$$\mathrm{Inv}(j_1 \otimes j_2 \otimes j_3 \otimes j_4) \neq 0. \tag{10}$$

In the recoupling channel $((j_1 j_2)k, (j_3 j_4)k)0$, this means that the allowed ranges for k overlap:

$$\max(|j_1 - j_2|, |j_3 - j_4|) \leq k \leq \min(j_1 + j_2, j_3 + j_4). \tag{11}$$

The overlap condition is just the polygon inequality on the four spins.

Proposition 2 (Closure–admissibility correspondence)**.** *Under the area-spin dictionary $A_f \propto j_f$, the following conditions are equivalent at a four-valent boundary node:*

(i) *the four face area-vectors can close;*

(ii) *the four areas satisfy the polygon inequality* (9)*;*

(iii) *the four-valent intertwiner space is non-empty.*

Thus the classical closure condition and the quantum admissibility condition are the same Gauss constraint expressed before and after quantisation.

Proof. Lemma 1 gives (i)⇔(ii). The recoupling range (11) is non-empty iff no spin is larger than the sum of the other three, which is (ii) with $A_f \propto j_f$. This proves (ii)⇔(iii). □

Remark 2 (What is, and is not, proved)*.* Proposition 2 is an area-vector statement. Full geometric reconstruction of a four-simplex also requires shape matching and consistent transport of bivectors between tetrahedral frames. Those are additional gluing data. The proposition establishes the first necessary bridge: the local closure constraint that makes a node geometric is exactly the local admissibility constraint that makes the spin-network amplitude non-zero.

4 The Lorentzian vertex and its booster

4.1 The boost as a bivector exponential

In the spacetime algebra, a boost of rapidity r in the 3-direction is generated by the bivector $\hat{\sigma}_3 = \gamma_3\gamma_0$,

$$x \longmapsto e^{-r\hat{\sigma}_3/2}\, x\, e^{r\hat{\sigma}_3/2}. \tag{12}$$

The Lorentzian EPRL vertex needs the corresponding unitary principal-series matrix element

$$d^{(\rho,k)}_{jl}(r; m) = \langle l, m | e^{-\imath r K_3} | j, m \rangle, \tag{13}$$

where $j = k, k+1, \dots$ and m is fixed by the boost along the 3-axis. The reduced matrix element is useful only if the generators really form a representation of $\mathfrak{so}(1,3)$.

Proposition 3 (Certified principal-series generators)**.** *A consistent Naimark-form implementation [15, 16] is obtained by taking*

$$B_j = \frac{k\rho}{j(j+1)}, \qquad \xi_j = \frac{1}{j}\sqrt{\frac{(j^2-k^2)(j^2+\rho^2)}{4j^2-1}}, \tag{14}$$

and

$$K_3|j,m\rangle = -mB_j|j,m\rangle - \imath\xi_j\sqrt{j^2-m^2}\,|j-1,m\rangle + \imath\xi_{j+1}\sqrt{(j+1)^2-m^2}\,|j+1,m\rangle, \tag{15}$$

with $K_\pm$ generated from commutators with K_3 rather than inserted by hand. On the interior of a finite $j_{\max}$ truncation the matrices satisfy

$$[K_i, K_j] = -\imath\epsilon_{ijk}J_k, \qquad [J_i, K_j] = \imath\epsilon_{ijk}K_k, \tag{16}$$

and the Casimirs are constant,

$$\vec{K}^2 - \vec{J}^2 = \rho^2 - k^2 + 1, \qquad \vec{J}\cdot\vec{K} = -k\rho. \tag{17}$$

The generator K_3 is Hermitian, so $e^{-\imath rK_3}$ is unitary and composes as a boost.

The essential numerical lesson is the one that fails most easily in direct implementations: the off-diagonal coefficient in (15) is imaginary while the diagonal coefficient is real. With the opposite choice, metric-looking identities can survive while the Lorentz commutators fail.

4.2 The node booster

The EPRL booster for a four-valent node is

$$B_4^\gamma(j_f, l_f; i, k) = \int_0^\infty \mathrm{d}r\, \sinh^2 r \sum_{\{m_f\}} I^i_{\{m_f\}}(j_f) \prod_{f=1}^{4} d^{(\gamma j_f, j_f)}_{j_f l_f}(r; m_f) I^k_{\{m_f\}}(l_f). \tag{18}$$

This is the standard booster decomposition of the Lorentzian EPRL amplitude [12, 11, 13, 14]. It separates the non-compact $\mathrm{SL}(2,\mathbb{C})$ part of the vertex from the $\mathrm{SU}(2)$ recoupling part.

Proposition 4 (Finite-cutoff booster evaluation)**.** *For fixed boundary spins, bulk spins, radial cutoff, and $j_{\max}$ truncation,* (18) *is a finite numerical integral. Increasing the radial cutoff and the spin truncation gives a convergence diagnostic for the computed booster. In the small-spin tests used here the on-shell channel $l_f = j_f$ carries the largest weight, but this dominance is treated as a numerical observation, not as a general theorem.*

The implementation uses the tridiagonal structure of K_3 at fixed m. This is both conceptually and computationally important: geometrically the boost is a bivector exponential; representation-theoretically it changes j by one unit while preserving m; numerically it reduces a dense diagonalisation on a space of size $O(j^2_{\max})$ to independent tridiagonal solves in the m sectors.

5 The four-simplex amplitude as a tensor network

5.1 The EPRL state sum

For the boundary graph K_5 of a four-simplex, the finite-cutoff EPRL vertex can be written as

$$A_v^\gamma(j_f, i_e) = \sum_{\{l_f \geq j_f\}} \sum_{\{k_e\}} \{15j\}(l_f, k_e) \prod_e B_4^\gamma(j_{f\supset e}, l_{f\supset e}; i_e, k_e), \tag{19}$$

where f labels the ten triangles and e labels the five boundary tetrahedra. The brute-force expression is correct but quickly becomes unusable: exciting all ten faces to $l_f = j_f, \ldots, j_f + l_{\text{cut}}$ has $(l_{\text{cut}}+1)^{10}$ bulk-spin configurations before the intertwiner and magnetic sums are considered.

The magnetic part has additional structure. A magnetic number m_f lives on each edge of K_5, while the four-valent intertwiner imposes one closure constraint at each node. The five constraints have rank four, leaving

$$b_1(K_5) = |E| - |V| + 1 = 10 - 5 + 1 = 6 \tag{20}$$

independent magnetic variables. This is the same graph-theoretic cycle number that organised the holonomies in the matter determinant of [1]. The two cycle spaces are not the same physical object–one carries magnetic labels, the other holonomies–but they are the same homological skeleton of the graph.

Proposition 5 (Cycle-space support)**.** *The magnetic sum in the K_5 spin-network evaluation of the $\{15j\}$ symbol can be parametrised by six independent edge magnetic numbers, one choice for each fundamental cycle after a spanning tree is fixed. Equivalently, four tree-edge magnetic labels are solved from node closure.*

5.2 Node tensors

The crucial improvement is to avoid treating $\{15j\}$, boosters, and the l-sum as separate nested loops. The node label k_e is local: it appears only in the booster of node e and in the node's four-valent intertwiner. Therefore its sum can be pushed inside the node. Bundle the bulk spin and magnetic number on each edge into a bond index

$$\alpha_f = (l_f, m_f), \qquad l_f = j_f, j_f + 1, \ldots, j_f + l_{\text{cut}}. \tag{21}$$

Then define the rank-four node tensor

$$T_e(\alpha_{f_1}, \ldots, \alpha_{f_4}) = \sum_{k_e} B_4^{\gamma}(j_{f\supset e}, l_{f\supset e}; i_e, k_e) I^{k_e}_{m_{f_1}\cdots m_{f_4}}(l_{f\supset e}) \times (\text{orientation phases}). \tag{22}$$

With these tensors the $\{15j\}$ is no longer computed separately; it is the wiring of the five node tensors.

Proposition 6 (Tensor-network EPRL vertex)**.** *The finite-cutoff vertex* (19) *is exactly the K_5 tensor contraction*

$$\begin{aligned} A_v^{\gamma} = \sum_{\{\alpha\}} & T_0(\alpha_{01}, \alpha_{02}, \alpha_{03}, \alpha_{04}) T_1(\alpha_{01}, \alpha_{12}, \alpha_{13}, \alpha_{14}) \\ & \times T_2(\alpha_{02}, \alpha_{12}, \alpha_{23}, \alpha_{24}) T_3(\alpha_{03}, \alpha_{13}, \alpha_{23}, \alpha_{34}) T_4(\alpha_{04}, \alpha_{14}, \alpha_{24}, \alpha_{34}). \end{aligned} \tag{23}$$

If all bonds have dimension $D = \sum_{l=j}^{j+l_{\text{cut}}}(2l+1)$, a hand-ordered node elimination contracts this network with peak arithmetic cost $O(D^8)$ and memory $O(D^6)$, rather than the $O(D^{10})$ scalar contraction of the naive magnetic sum.

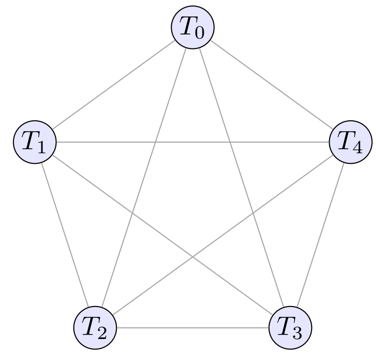

five rank-4 node tensors $T_e = \sum_k B_4^\gamma I^k$,
one bond $\alpha = (l, m)$ per triangle, contracted on K_5

Figure 2: Tensor-network form of the four-simplex vertex. Each tetrahedron is a rank-four tensor fusing the Lorentzian booster and the four-valent intertwiner; each triangle is a shared bond.

5.3 The semiclassical phase

For non-degenerate Lorentzian boundary data, the large-spin asymptotics of the EPRL four-simplex amplitude contains phases proportional to the Lorentzian Regge action [9, 17, 10],

$$S_{\text{Regge}} = \sum_t A_t \Theta_t. \tag{24}$$

Here the areas A_t and dihedral angles Θ_t are precisely the geometric data reconstructed from the bivectors. The paper does not numerically take the large-spin limit; it only identifies the classical Regge functional supplied by the spacetime-algebra reconstruction and shows where it enters the known asymptotic structure of the Lorentzian vertex.

6 Discussion

The companion paper left a precise gap: its matter-built graph carried Lorentz frames, cycle holonomies, simple tetrad blades, and a determinant-induced field equation, but it did not yet explain how those ingredients become the simplicity-constrained data of a spin-foam vertex. The present paper fills that gap at the finite-complex level.

The first result is conceptual. The two invariants used to classify matter-built curvature bivectors are the same two invariants carried by the EPRL representation labels, modulo conventional signs. Linear simplicity is therefore not an unrelated condition; it is a distinguished ray in the invariant plane already used by the matter-first construction. The second result is kinematical. Closure of four area-vectors, the Minkowski polygon inequality, and the non-emptiness of the four-valent intertwiner space are equivalent. This is the local point at which a classical tetrahedron and a quantum spin-network node meet. The third result is algorithmic. The Lorentzian EPRL vertex can be assembled from a certified principal-series boost, a finite node booster, and a K_5 tensor-network contraction. The graph cycle structure that controlled the matter determinant reappears as the support of the magnetic spin-network sum.

The limitations are equally important. First, the closure-admissibility result is local and area-vector based; full four-simplex reconstruction additionally requires shape matching and consistent bivector transport. Second, the booster construction is certified internally by algebra closure, Casimirs, boost composition, and convergence tests, but it still needs independent numerical cross-checks. Third, the tensor-network contraction evaluates a finite-cutoff vertex; it is not a renormalised spin-foam model and does not prove a continuum limit. Fourth, the Regge action is identified through the known asymptotic structure of the EPRL vertex, not extracted here by a large-spin numerical limit.

These limitations point to the next tasks. The most immediate is an independent small-spin benchmark of the booster and vertex values against published reference values or an independently implemented code path. The second is a sparse or path-optimised version of the K_5 tensor network, needed for larger l_{cut} and non-uniform boundary spins. The third is a two-vertex or Pachner-move experiment comparing a glued complex with an effective single vertex. That would bring the determinant RG of [1] and the EPRL amplitude into the same numerical coarse-graining problem.

What has been established here is therefore deliberately modest but structurally useful: the matter-first graph, the bivector simplicity constraints, and the finite Lorentzian four-simplex amplitude can be written in a common $\mathrm{Cl}(1,3)$ and cycle-space language. This makes the programme concrete enough to test rather than only interpret.

Acknowledgements

The author thanks the developers of the spacetime-algebra, spin-foam, tensor-network, and numerical EPRL traditions on which this work builds. Any remaining errors in the bridge proposed here are the author's responsibility.

References

[1] G. Utama, "Matter-First Dynamics in LQG: Fermion Determinants, Spacetime-Algebra Tetrads, and an Induced Discrete Field Equation," ai.viXra.org:2606.0064 (2026), https://ai.vixra.org/abs/2606.0064.

[2] R. Penrose, "Angular momentum: an approach to combinatorial spacetime," in *Quantum Theory and Beyond*, ed. T. Bastin (Cambridge University Press, 1971), pp. 151–180.

[3] M. Altaisky, "Combinatorial spacetime from loop quantum gravity," arXiv:2602.08341 [gr-qc] (2026).

[4] C. Rovelli and F. Vidotto, *Covariant Loop Quantum Gravity* (Cambridge University Press, 2014).

[5] J. Engle, E. Livine, R. Pereira, and C. Rovelli, "LQG vertex with finite Immirzi parameter," Nucl. Phys. B **799**, 136 (2008).

[6] J. W. Barrett and L. Crane, "Relativistic spin networks and quantum gravity," J. Math. Phys. **39**, 3296 (1998).

[7] A. Barbieri, "Quantum tetrahedra and simplicial spin networks," Nucl. Phys. B **518**, 714 (1998).

[8] J. C. Baez and J. W. Barrett, "The quantum tetrahedron in 3 and 4 dimensions," Adv. Theor. Math. Phys. **3**, 815 (1999).

[9] G. Ponzano and T. Regge, "Semiclassical limit of Racah coefficients," in *Spectroscopic and Group Theoretical Methods in Physics* (North-Holland, 1968), pp. 1–58.

[10] J. W. Barrett, R. J. Dowdall, W. J. Fairbairn, F. Hellmann, and R. Pereira, “Lorentzian spin foam amplitudes: graphical calculus and asymptotics,” Class. Quantum Grav. **27**, 165009 (2010).

[11] P. Donà, M. Fanizza, G. Sarno, and S. Speziale, “Numerical study of the Lorentzian Engle–Pereira–Rovelli–Livine spin foam amplitude,” Phys. Rev. D **100**, 106003 (2019).

[12] S. Speziale, “Boosting Wigner’s nj-symbols,” J. Math. Phys. **58**, 032501 (2017), arXiv:1609.01632.

[13] F. Gozzini, “A high-performance code for EPRL spin foam amplitudes,” Class. Quantum Grav. **38**, 225010 (2021), arXiv:2107.13952.

[14] P. Donà and P. Frisoni, “How-to compute EPRL spin foam amplitudes,” Universe **8**, 208 (2022), arXiv:2202.04360.

[15] M. A. Naimark, *Linear Representations of the Lorentz Group* (Pergamon, 1964).

[16] W. Rühl, *The Lorentz Group and Harmonic Analysis* (Benjamin, 1970).

[17] T. Regge, “General relativity without coordinates,” Nuovo Cim. **19**, 558 (1961).

[18] D. Hestenes, *Space–Time Algebra* (Gordon and Breach, 1966).

[19] C. Doran and A. Lasenby, *Geometric Algebra for Physicists* (Cambridge University Press, 2003).

[20] A. D. Sakharov, “Vacuum quantum fluctuations in curved space and the theory of gravitation,” Sov. Phys. Dokl. **12**, 1040 (1968).